A model for manufacture of nano-sized smart materials free from impurities†

N. Rudraiah[1,*] and Chiu-on Ng[2]

[1]National Research Institute for Applied Mathematics, 492/G, 7th Cross, 7th Block (West), Jayanagar, Bangalore 560 070, India and UGC–CAS in Fluid Mechanics, Department of Mathematics, Bangalore University, Bangalore 560 001, India
[2]Department of Mechanical Engineering, The University of Hong Kong, Pokfulam Road, Hong Kong, Peoples Republic of China

The importance of nano-sized smart materials in structural engineering, biomedical engineering, and in military applications is discussed. It is shown that the solidification of poorly conducting alloys involved in the manufacture of these materials gives rise to surface and convective instabilities. Different types of surface and convective instabilities are briefly discussed. These instabilities produce a mushy zone regarded as dendrites of nano-sized crystals. These dendrites arising from instabilities are regarded as impurities. To manufacture nano-sized smart materials free from impurities, it is essential to control both surface and convective instabilities. We discuss here briefly, different types of convective and surface instabilities in a poorly conducting fluid. We also discuss different mechanisms of control of these instabilities. Different analytical and numerical techniques used to investigate these instabilities under different boundary conditions are discussed. In this review the moment method is explained to find the condition for the onset of convection, and porous lining is used to suppress the growth rate of surface instability. This is useful in the manufacture of nano-sized smart materials free from impurities. Different methods to obtain the required basic equations and the corresponding boundary conditions are briefly discussed.

AN important challenge in nanotechnology, which at present is the most energized discipline in science and technology is to manufacture new materials involving sensing and actuating properties, like smart materials, shape memory alloys (SMA), etc. because of their applications in quantum computers, civil (biomechanical, structural engineering, etc.) and in military applications. The important process in the manufacture of these nano-materials is the solidification of alloys like nickel–titanium, aluminium oxide, etc. by cooling from below and heating from above. At present, ferroelectric alloys have been widely used in making smart devices[1,2] of ferroelectrics. A poorly conducting alloy, where the electrical conductivity σ is a strong function of temperature T, can also be used to manufacture smart materials. However, little is known about the use of poorly conducting alloys to manufacture smart materials. In this review, we concentrate on nano-materials made of alloys having poor electrical conductivity. The physical mechanism here is as follows.

The difference in σ due to difference in T induces free charges, ρ_e, in the bulk of the fluid as well as at the interface. These free charges interacting with either induced, applied or both induced and applied electrical field, $\vec{E}$, produce a force $\rho_e\vec{E}$. This force, like buoyancy force, produces the following two types of instabilities: (i) Convective instability known as electroconvective instability and (ii) surface instabilities, called electrosurface instability.

Different types of convective and surface instabilities and causes for these instabilities are discussed below.

Convective instability

The following kinds of convective instabilities, also known as convection, have been extensively investigated.

Rayleigh–Benard convection

Convection in a horizontal layer of a Boussinesq fluid heated from below and cooled from above in the presence of gravity is called Rayleigh–Bernard convection. The cause for this convection is the buoyancy force arising due to the variation of density of fluid with temperature in the presence of gravity.

Oberbeck convection

Convection in a vertical layer of Boussinesq fluid heated and cooled from sides, maintaining temperature difference perpendicular to gravity is called Oberbeck convection[3]. The cause for this convection is also buoyancy force.

Magnetoconvection

Convection in a horizontal layer of Boussinesq electrically conducting fluid in the presence of a magnetic field, transverse or horizontal, and gravity is called magneto-

†This article is part of the William Mong Research Fellowship Award Lecture 2002–2003 delivered by N. R. on 11 July 2003 at the Department of Mechanical Engineering, The University of Hong Kong, Hong Kong.
*For correspondence. (e-mail: nrudraiah@hotmail.com)

convection (MTC). The cause for MTC is the combined effects of buoyancy force and Lorentz force in the presence of a magnetic field. The effect of magnetic field is to set up overstable motion, i.e. principle of exchange instability is valid[4–6] for certain values of Chandrasekhar number and suppresses convection. However, in the case of two components of an electrically conducting fluid, like temperature and concentration, Rudraiah and Shivakumara[7] have shown that for a certain frequency range, the magnetic field augments convection instead of suppressing it.

Marangoniconvection

Convection in a horizontal layer of Boussinesq fluid, where at least one of the bounding surfaces of the fluid is free with surface tension, heated from below and cooled from above is called marangoniconvection (MC). The cause for MC is the variation of surface tension with temperature, which produces the surface tension-driven convection or MC[5,8–11].

Magneto-Marangoniconvection

Convection in a horizontal layer of an electrically conducting Boussinesq fluid bounded at least on one side by a free surface subjected to surface tension, heated from below and cooled from above in the presence of a magnetic field and surface tension is called Magneto-Marangoniconvection (MMC). The cause for MMC is the combined effect of variation of surface tension with temperature and magnetic field. Here also, the effect of magnetic field is to suppress MC and it facilitates the principle of exchange of stability to be valid under certain conditions[12,13].

Magnetic fluid convection

Magnetic fluids are electrically non-conducting colloidal suspension of tiny particles of solid ferromagnetic material in a non-electrically conducting carrier fluid like water, kerosene, hydrocarbon, etc. These behave as homogeneous continuous fluids and are not found in nature, but are artificially synthesized. Like dielectric polarization in electric materials, there exists magnetic polarization in magnetic materials. The magnetic polarization per unit volume is called magnetic moment. This magnetic moment is a strong function of magnetic field and temperature.

Convection in a horizontal layer of Boussinesq magnetic fluid in the presence of buoyancy force and magnetic field, heated from below and cooled from above is called magnetic fluid convection (MFC) or ferroconvection (FC). The cause for MFC is the variation of magnetization with magnetic field and temperature, in addition to variation of density with temperature[14].

Marangoni magnetic fluid convection

Convection in a horizontal layer of Boussinesq magnetic fluid bounded at least on one side by a free surface with surface tension in the presence of a magnetic field, heated from below and cooled from above is called Marangoni magnetic fluid convection (MMFC). The cause for MMFC is due to the combined effect of variation of surface tension with temperature and variation of magnetic moment with magnetic field and temperature. This is of vital importance in space research because it facilitates cooling of machineries[15,16].

Electroconvection

Convection in a horizontal layer of a poorly conducting fluid, in the presence of an applied electric field and buoyancy force, cooling from below and heating from above produces electroconvection (EC).

Here, the physical mechanism is the variation of electrical conductivity of fluid, σ, with temperature producing free charges in the bulk of the fluid as well as at the surface. These free charges interacting with the applied or self-generating electric field produce a force. This force generates a convection called electroconvection (see refs 17–20 and references therein).

Oberbeck electroconvection

Convection in a vertical layer of a poorly conducting fluid in the presence of electric field and buoyancy force, where the temperature difference is maintained normal to gravity produces Oberbeck electroconvection.

Marangoni electroconvection

Convection in a horizontal layer of a poorly conducting Boussinesq fluid bounded at least on one side by a free surface with surface tension, cooled from below and heated from above in the presence of an electric field is called Marangoni electroconvection (MEC). The physical mechanism here is the variation of both surface tension and electrical conductivity with temperature in the presence of an electric field which produces convection as explained above. This convection is called Marangoni electroconvection[21,22].

Different analytical and numerical techniques[23,24] have been extensively used to study the onset of convection and the corresponding heat and mass transfer.

Surface instabilities

Surface instabilities play a significant role in solidification processes, inertial fusion energy (IFE), cooling of

machineries, etc. Therefore, in this section we briefly discuss different types of surface instabilities.

Rayleigh–Taylor instability

Rayleigh–Taylor instability (RTI) occurs due to superposition of two fluids of different densities. For example, instability of the interface of a heavy fluid that rests above a lighter fluid is known to overturn under the action of gravity. This surface instability arising not only when a heavy fluid is supported by a lighter fluid, but also when a dense material is accelerated by a less dense material is called RTI[4,25–29].

Kelvin–Helmholtz instability

The second kind of instability arises when different layers of homogeneous or stratified heterogeneous fluid are in relative horizontal motion. A speciality here is when two superposed fluids flow one over the other with a relative horizontal velocity, the instability of the plane interface between the two fluids when it occurs in this situation, is called Kelvin–Helmholtz instability (KHI). The cause for KHI is the shear that develops at the interface due to different velocities of two superposed fluids[30–32].

Richtmyer–Meshkov instability

The third type of surface instability arises due to the effect of shock accelerating a perturbed interface between two fluids of different densities. In some cases, part or all of the acceleration is impulsive, that is, $g(t)$ is very large during a very short time interval and zero or small outside the interval. The limiting case of impulsive acceleration is accelerated by a shock where the compressibility of the fluid cannot be neglected. The surface instability when a shock sweeps across a corrugated interface from a less dense to a more dense fluid is called Richtmyer–Meshkov instability[33,34].

Saffman–Taylor interface instability

Saffman and Taylor constructed a Hele-Shaw cell model for a porous media filled with oil. By suitable means, they applied water under pressure. At one end of the cell, oil was driven out ahead of water. While some of the oil was squeezed out in this fashion, the water also penetrated the cell as a finger having rounded advancing tip along sides parallel to the edges of the channel, where the shape of the meniscus profile between the oil and the water has narrow thickness of the shell. In that case, Saffman and Taylor found that the asymptotic width of the finger far from the advancing tip was never less than half the width of the channel for slow rates of advance, almost all the cell contents were swept out and as the speed of the finger was increased due to the increasing pressure applied to the penetrating fluid, the width steadily approached the limiting value of one of the channel widths. Here the oil drives the water out of a long, straight channel of small thickness formed between two parallel sheets scaled at the edges. The penetrating fluid forms a long finger whose sides are parallel to the edge of the channel and which has a rounded tip that advances with unaltered shape at a constant speed U. The long finger of penetrating fluid is called Saffman–Taylor surface instability[32].

Motivation of this review

Solidification process in the manufacture of new materials like smart materials involves a mushy layer. A phenomenon commonly associated with the evolution of the mushy layer is the occurrence of chimneys which are cylindrical holes free of solids that have formed spontaneously[15]. These are also called dendrites or freckles. These dendrites can be regarded as a porous layer with perfect spacing between the mushy streaks. This mushy zone, a region of mixed solid and liquid phase, is separated by a thin film having an interface between them.

The study of instability of the interfaces is of fundamental importance in recent years in view of its significant role in understanding the control and exploitation of many of the basic physical, chemical and biological processes. The interfaces in some of these instances occur due to the following physical phenomena.

The solidification process produces dendrites or freckles as explained above, which are regarded as impurities. Therefore, to manufacture these strong materials free from impurities in microgravity environment, we have to study both surface instabilities and electroconvection in a poorly conducting fluid-saturated porous layer. Such a study is important in the manufacture of SMA free from impurities because of its applications in civil and military fields, as explained below.

Civil applications

Smart structures: Engineers are constructing smart buildings with self-adjusting windows and self-cleaning materials. These smart materials have also become attractive for other structural applications. These smart materials develop mechanical response under non-mechanical stimuli, such as electric fields and can be embedded or attached to the composite materials to create a facility to sense the current stress state in composite materials, like laminate, and to introduce modifications to the stress state to mitigate the possibility of failure. Such structures which have in-built sensing, actuation and control features are known as smart structures. With such features inherent in the structures, it is possible to design them to

achieve several performance advantages such as high level of safety, reduced vibration, reduced noise, high shape control with accompanying pay-offs in relation to durability and economic gains. It is important to keep in mind that mechanics of structural failures do occur and this issue is of paramount concern in structural engineering. Here, smart structures are of significant importance because, with the help of smart materials, it is possible to monitor stress situation and the possibility of failure, which are revealed on-line so that corrective actions can be initiated to avoid the risk of failure. These structures will have an in-built control system which, in case of need, introduces a corrective stress system to automatically mitigate the effect of damage due to specially built-in smart patches. Thus we will have structures manufactured by smart materials with smart patches that may prevent failures.

Another important application of smart structures is automatic reduction of vibration levels in structural components. With the help of appropriate actuation strains through smart patches, the vibrating environment can be significantly reduced if not eliminated all together. With the help of these smart materials with appropriate smart patches it would be possible to build platforms that do not vibrate, antenna that do not deviate from the chosen target or airplane wings that do not experience vibration.

Biomechanical and biomedical engineering applications

(i) Smart materials are useful for diabetics to sense sugar levels and deliver insulin.
(ii) SMA smart materials are successful in the use of orthodontic arch wires in dentistry. These wires will make the misaligned teeth gradually return to their original shape, exerting a small and nearly constant force on the misaligned teeth. The use of these smart wires reduces patient discomfort and helps in efficient and faster tooth movement.
(iii) SMA smart materials are also used as blood-clot filters. These SMA smart materials involve the use of titanium–nickel wires that are first trained to clot blood trapping coiled configuration prior to the insertion of the cooled straightened wire. The wire is inserted into the vena cava, where due to the heat caused by blood flow, the original blood-clot filtering configuration is reverted to.
(iv) The constriction of arteries due to the plaque, called stenosis, restricts blood flow so that cardiologists have to often resort to bypass surgery and this can be avoided by the smart implants.
(v) A concept of smart healing is being evolved by implementing piezo poly-vinylidiene fluoride (PVDF) based sensor in the jaw. This would generate an electric field every time the patient bites on it and this electric field would promote the healing process. We note that PVDF is used in transportation, for sensing traffic either by registering vibrations or by measuring the heat generated by automobiles.

Military applications

The Air Force requires smart planes for the following purposes: (i) Minimizing the weight and maximizing strength of the planes. (ii) Planes that can continuously change their wing shape to achieve supersonic speed and evade radar screen.

The two types of instabilities discussed in the beginning of this section produce impurities known as plumes, streaks or freckles made of nano-particles. These impurities produced as end-products are inevitable in nanotechnology in the manufacture of strong materials. Therefore, to manufacture these strong materials with nano-sized porous layer free from impurities, we have to understand: (i) surface instability of RT-type involving a composite layer made of partly a nano-sized porous layer and partly a thin layer of fluid and (ii) convection in a nano-sized porous layer.

Controls of these two types of instabilities are essential in the manufacture of nano-sized smart materials. Before illustrating these problems, we briefly discuss the required basic equations.

Basic equations

Liquid-to-solid transformation, in particular, the effect of mass transport on growth, behaviour and morphological evolution gives rise to dendrites, regarded as nano-sized porous media having uniform spacing. The question is how to model this liquid alloy flow in the nano-sized porous media. The best thing, because of microspacing, is to formulate the problem considering a molecular picture involving force of attraction and repulsion using one of the following statistical averages: (i) volume averaging procedure or (ii) ensemble averaging procedure.

These averages are needed because, in general, it is impossible to know what is happening in each of the many nano-pores, hereafter called pores, between many nano-particles. Here, the best one can expect is knowledge of the above statistical averages of the physical quantities over certain representatives of the system.

Volume averaging procedure

Following the work of Rudraiah[15], we briefly explain here the basic concepts of the averaging procedure. For details, one can also refer to the books of Kaviany[35] and Nield and Bejan[36].

Consider a representative volume ΔV that is large compared with the pore size of the material consisting of

nano-particles but small compared with the characteristic length.

Let

$$\varepsilon = \frac{\text{volume of void space of nano-particles}}{\text{total volume}},$$

be the effective porosity of ΔV.

Let $f(x_i)$ be some properties of the fluid alloy, which by definition are zero in the case of solid nano-particles. Then the pore volume average of f is defined as

$$\langle f \rangle^* = \frac{1}{\varepsilon \Delta V} \int_{\varepsilon \Delta V} f \, \mathrm{d}V.$$

The bulk volume average of f is defined as

$$\langle f \rangle = \frac{1}{\Delta V} \int_{\varepsilon \Delta V} f \, \mathrm{d}V = \varepsilon \langle f \rangle^*.$$

These averages can be viewed as point macroscopic quantities associated with the centroid of ΔV, which may lie either in a pore or on a solid portion of nano-sized porous medium. In other words; $\langle f \rangle$ and $\langle f \rangle^*$ are defined at each point in a fictitious continuum representing the fluid-saturated void of the medium consisting of nano-particles, and their values may thus change from point to point within a given ΔV. The general Reynolds transport theorem relates the average of the gradient equal to gradient of the average according to

$$\left\langle \frac{\partial f}{\partial x_i} \right\rangle = \frac{\partial}{\partial x_i} \langle f \rangle + \frac{1}{\Delta V} \int_s f \, \hat{n}_i \, \mathrm{d}s,$$

where s is the solid–fluid interface in ΔV and $\hat{n}_i$ are the components of unit normal vector pointing in the direction of the nano-solids.

Using these volume averages, we can derive the required basic equations incorporating the forces of attraction and repulsion.

Ensemble averaging procedure

We can assume nano-particles in a fluid medium to be in the form of spheres and define the ensemble average of a dynamical system, say ϕ, as

$$\langle \phi \rangle = \int P(\chi, r) \phi(\chi, r) \mathrm{d}\chi \, \mathrm{d}r,$$

where $\chi = \chi_1, \chi_2, \ldots, \chi_N$ (N is large) are positions of the nano-particles, $r = r_1, r_2, \ldots, r_N$ are the radii of these nano-particles, P is the probability of finding the system in the known state. Assuming random distributions of nano-particles, the density distribution can be written as

$$n(\chi, \sigma) = NP(\chi, \sigma),$$

where $n(\chi, \sigma)\mathrm{d}\sigma$ is the fraction of number density of nano-particles with radii between r and $r + \mathrm{d}r$ in the neighbourhood of χ.

In addition to this, to derive the required basic equations for flow through the voids, we have to use the point force approximations:

(i) The disturbance produced by a nano-particle is to be approximated by that of a point-force located at the centre of the nano-particle. This force may be equal in magnitude but opposite in direction to the drag on the particle.

(ii) The drag experienced by a nano-particle is approximately directly proportional to the undisturbed velocity of the fluid at the centre of the particle. This includes the fluid velocity in the absence of all nano-particles and the perturbed fluid velocities due to all other nano-particles. This approximation implies that

$$\text{Drag} = D(r) q_i(x),$$

where q_i is the unperturbed fluid velocity at the centre of the nano-particle and $D(r)$ is a coefficient which depends on the size of the nano-particle and statistical properties of the N nano-particles. The crux of the problem here is to find the dependence of D on r. This can be found using the point force approximation (i) given above. In these approximations, the velocity and pressure at a point χ can be written as

$$q_i(\chi) = q_i^0(\chi) - \sum_{n=1}^{N} G_i^n(r_n, \chi_n) q_{ij}(\chi, \chi_n),$$

$$P(\chi) = p^0(\chi) - \sum_{n=1}^{N} G_i^n(r_n, \chi_n) P(\chi, \chi_n),$$

where i and j denote the vectors, $q_i^0(\chi)$ and $\rho^0(\chi)$ are the fluid velocity and pressure in the absence of nano-particles, G_i^n is the drag on the nano-particle n in the ith direction and q_{ij} is the velocity of fluid in the ith direction at χ due to the point-force of unit strength in the jth direction at χ_n. To derive the required equations we assume

$$G_i^n = D(r_n) q_i^n(x_n),$$

$$q_i^n(x_n) = q_i^0(x) - \sum_m {}^1 G_j^m \, q_{ij}(x, x_m),$$

where $\sum^1$ means the term $m = n$ is excluded from the summation. That is, $q_i^n(\chi_n)$ is the unperturbed fluid velocity as seen by the particle n.

Taking the ensemble average of these over the configuration space, we can derive the basic equations[34].

Basic equations for composite media

Following one of the above procedures, we can obtain the required basic equations.

The conservation of momentum

$$\bar{\rho}\,[\times_p(\varepsilon^{-1}-1)+1]\frac{\partial\vec{q}}{\partial t}+\rho\,[\times_p(\varepsilon^{-2}-1)+1]\,(\vec{q}.\nabla)\,\vec{q}$$

$$=-\nabla p+\mu\left[\times_p\left(\frac{\bar{\mu}}{\mu}-1\right)+1\right]\nabla^2\vec{q}-\times_p\left[\frac{\mu}{k}+\frac{\rho C_b}{\sqrt{k}}|\vec{q}|\right]\vec{q} \tag{1}$$

where

$$\times_p=\begin{cases}1 & \text{for porous media}\\ 0 & \text{for fluid region.}\end{cases}$$

and C_b is drag coefficient.

The conservation of mass for Boussinesq fluid:

$$\nabla\cdot\vec{q}=0, \tag{2}$$

where

$$\bar{\rho}=\rho_f\left[1+\times_p\left(\frac{\rho_p}{\rho_f}-1\right)\right]=\text{density},$$

$$\bar{\mu}=\mu_f\left[1+\times_p\left(\frac{\mu_{ef}}{\mu_f}-1\right)\right]=\text{viscosity},$$

μ_f is viscosity of fluid, μ_{ef} is effective or Brinkman viscosity and suffixes p and f denote quantities in porous lining and in the fluid film, respectively. These equations have to be supplemented with suitable boundary and interface conditions given below.

Boundary conditions

The boundary conditions on velocity will depend on the following configurations.

Rigid boundaries: If (u, v, w) are the components of velocity of the fluid, then in the case of fluid bounded by rigid boundaries, using the conservation of mass, the no-slip conditions at the rigid boundaries are

$$W=\frac{dW}{dz}=0. \tag{3}$$

Stress-free boundaries: In this case in the absence of surface tension, the boundary conditions are

$$W=\frac{d^2W}{dz^2}=0. \tag{4}$$

Free-surface with surface tension: In this case the surface tension γ is a function of temperature. Following Pearson[8] one usually observes that γ varies linearly with temperature and the boundary conditions are:

$$W=\frac{d^2W}{dz^2}-M_a\theta=0, \tag{5}$$

where M_a is the Marangoni number given by

$$M_a=\frac{\gamma_T\,\Delta Th}{\mu_f\kappa},$$

κ is the thermal diffusivity, ΔT is the temperature difference between the lower heated surface and the cooled upper surface and γ_T is the gradient of surface tension with temperature.

Bounded by densely packed porous layer: In this case, Beavers and Joseph[37] postulated a slip-boundary condition

$$\frac{du}{dy}=\frac{\alpha\,(u_B-Q)}{\sqrt{k}}, \tag{6}$$

where u is the horizontal velocity in the x-direction, u_b is the slip at the nominal surface, Q is the Darcy velocity, y is the vertical coordinate, k is the permeability of the porous medium and α is the slip parameter. The condition (eq. (6)) is called Beavers and Joseph (BJ)-slip condition.

The BJ-slip condition (eq. (6)) is independent of the depth, say h, of fluid. Later Rudraiah[38] derived the slip-boundary condition in the form

$$\frac{du}{dy}=\left(\frac{\lambda}{k}\right)^{i/2}\left[\frac{\varepsilon\lambda\,u_m}{sh\delta\,h}+(u-u_m)\,cth\delta h\right]. \tag{7}$$

This condition depends on the depth of fluid h and hence is valid in many industrial and biochemical problems. Here λ is a viscosity parameter, $\delta=(\lambda k)^{-0.5}$ and u_m is the slip velocity at the nominal surface.

We note that the BJ-condition (eq. (6)) can be obtained as a particular case from the Rudraiah condition (eq. (7)) as $h\to\infty$ and hence the condition (eq. (7)) is called BJR-condition.

Bounded by sparsely packed porous layer: Here, the fluid flow is governed by the Brinkman equation analogous to

the Navier–Stokes equation. In that case, the condition will depend on the assumption of (i) nominal surface or (ii) the usual surface. The nominal surface is derived as a smooth geometrical surface drawn in the fluid such that the outermost perimeters of all surface pores of the permeable material are on this surface.

In the case of nominal surface, even in the case of sparsely packed porous layer BJR-slip condition (eq. (7)) is valid.

If the interface between the fluid-saturated porous layer and the thin film is a usual surface instead of a nominal surface, then we have to impose the residual shear condition

$$\mu_{ef}\frac{\partial u_p}{\partial y}-\mu\frac{\partial u}{\partial y}=\frac{\alpha_p}{\sqrt{k}}\mu u_p, \tag{8}$$

where α_p is the residual slip coefficient and μ_{ef} is the effective (i.e. Brinkman) viscosity.

Rough rigid surface condition: In this case we specify the condition[39]:

$$\frac{du}{dy}=\alpha_r u, \tag{9}$$

where α_r is the roughness parameter.

Isothermal condition: In the case of boundaries maintained at constant temperature T_i ($i = L$, lower boundary and $i = U$, upper boundary), we specify the boundary condition on temperature as

$$T = 0, \tag{10}$$

where T is the difference in temperature.

Adiabatic condition: In the case of boundaries maintained at constant heat flux called adiabatic boundaries, we specify

$$DT = 0. \tag{11}$$

Radiation condition: In the case of general radiation case, we specify

$$DT + \lambda_b T = 0, \tag{12}$$

at the boundaries. The condition (eq. (12)) is called radiation boundary condition, and λ_b will be connected to the Biot number.

In addition to the above boundary conditions, we have to impose the following dynamical and kinematical conditions in the study of surface instabilities.

Dynamic condition: In the case of two-dimensional flow of velocity components (u, v) in x and y directions, we impose the following dynamic condition:

$$p=-\delta\eta-\gamma\frac{\partial^2\eta}{\partial x^2}, \tag{13}$$

where p is the pressure, $\delta = g(\rho_p - \rho_f)$ is the normal stress, γ is the surface tension and η is the elevation of the interface.

Kinematics condition:

$$v=\frac{\partial\eta}{\partial t}+u\frac{\partial\eta}{\partial x}. \tag{14}$$

Mechanisms to control convective instabilities

As explained earlier, the layers of dendrites of nano-size (Figure 1) resulting from solidification of alloys in materials processing are regarded as impurities. To control these impurities, it is essential to control convective instabilities in the presence of dendrites regarded as porous layers because of uniform spacing between nano-sized dendrites. Microgravity environment, Coriolis force, Lorentz force, electric force, concentration flux, non-uniform temperature gradient and time-variant electric field are used in the literature to control convective instabilities. For details see the work of Rudraiah *et al.*[39].

Mechanism to control surface instabilities

As stated earlier, solidification process in the manufacture of nano and smart materials and also the laser beam in the case of IFE target produce surface instabilities of the types discussed above. These surface instabilities give rise to impurities due to manufacturing processes involved in nano and smart materials and cause asymmetry in the IFE target. Therefore, to manufacture nano and smart materials free from impurities and to maintain symmetry in IFE target, it is important to control these

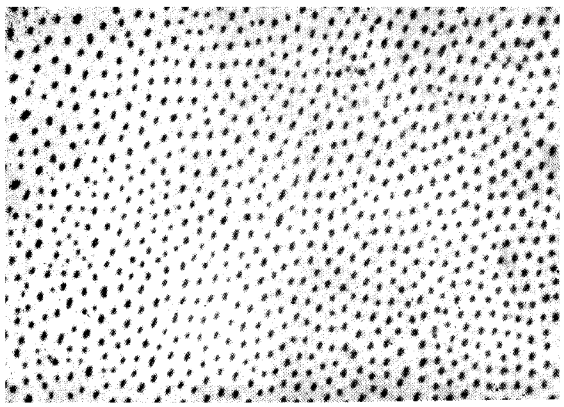

Figure 1. Transverse microstructure of Al–Ni (Al–Al_3 Ni) eutectic alloy.

instabilities. Heterogeneous or compressible in viscid fluid, foam material, nano-structured lining, external constraint of transverse magnetic field, external constraint of transverse electric field, surface tension effect, rough and coated interface are effective in controlling these instabilities. For details see the work of Rudraiah[28].

In the remaining part of this review we briefly discuss the effect of oscillatory electric field on the control of EC in a mushy layer made up of nano-sized dendrites. Next we discuss the effect of porous lining on the control of RTI.

Effect of oscillatory electric field on the control of EC in mushy layer made up of nano-sized dendrities

The study of electro-thermal convection (ETC) in a mushy layer saturated with a poorly conducting ohmic fluid in the presence of steady or unsteady and uniform or spatial variation of electric field is sparse, in spite of its application in the solidification process involved in the manufacture of nano, smart and other materials. The ETC of a plane, horizontal, poorly conducting ohmic liquid in a steady electric field, has been investigated experimentally[40,41] and theoretically[40–42]. Turnbull[40] and Lee *et al.*[41] have shown that under several assumptions on the physical properties of a poorly conducting liquid, oscillatory instability of the layer heated from above is possible. Lee[42] has also studied the influence of the time relaxation of electric charges on ETC. These works on ETC were mainly concerned with charge creation due to the time-dependent electrical conductivity of the liquid, neglecting non-uniform polarization of the liquid and charge injection. This is justified in view of the physical properties of the liquid and materials of the electrodes used in their experimental and theoretical work. Recently, Smorodin and Velarde[43] have studied ETC in the presence of a vertical time-varying electric field in a horizontal layer of a poorly conducting liquid. They have shown the existence of unstable disturbances due to the frequency of applied electric field as well as due to the intrinsic frequency of neutral disturbances of steady electric field in a poorly conducting ohmic liquid. In particular, they have shown that this behaviour is opposite to the results of finite frequency vibrations or time-varying electric fields, when the response time period of the liquid system coincides or is twice the external modulation period. Smorodin and Velarade[43] have also shown that depending on the amplitude and frequency of modulation, the electric field can stabilize an unstable base state or destabilize the equilibrium of the liquid.

The works mentioned above are concerned with poorly conducting ohmic liquid in a pure liquid layer, i.e. in the absence of a mushy layer regarded as the liquid-saturated porous layer. The study of ETC in such a mushy layer, i.e. porous layer, is important in the manufacture of nano and smart materials[28]. In spite of this, the ETC in a porous layer has not been given much attention. It is known[28] that under certain conditions on electric Rayleigh number, oscillatory ETC are possible modes. In particular, it has been shown that the effect of electric field stabilizes marginal state (i.e. neutral state) and destabilizes oscillatory (i.e. over stable) state[43]. It is of importance, as in the case of non-uniform temperature gradient, to know whether a nonuniform electric field controls ETC in a porous layer, which is of importance in the manufacture of nano and smart materials.

Mathematical formulation

We consider an infinite horizontal fluid-saturated porous layer bounded by rigid, thermal and electroconducting plates embedded with electrodes located at $z = \pm h$ (Figure 2). Constant but different temperatures $T = \mp \theta_1$ and different electric potentials $\phi(+h) - \phi(-h) = -2V(\eta_1 + \eta_2 \cos\Omega t)$ are maintained on these boundaries. Here V is the characteristic voltage applied between the embedded electrodes; η_1 and η_2 are respectively, the amplitudes of steady and modulated components of potential, and Ω is the modulation frequency. The modulation amplitude η_2 varies continuously, whereas η_1 takes only two values, namely $\eta_1 = 0$ for alternating potential difference and $\eta_1 = 1$ for the steady modulations of the background[43]. In this review, we use the electro hydrodynamic (EHD) approximations, namely the electric conductivity. σ_e of the liquid is negligibly small (because we consider a poorly conducting liquid), so that the induced magnetic field is negligible. This approximation makes the electric field $\vec{E}$, to be conservative, i.e. $\vec{E} = -\nabla\varphi$. Further, it limits the frequency of the electric field and electrical conductivity of the liquid, that is

$$\frac{\Omega}{2\pi} \ll \frac{c}{h}, \quad \sigma_e \ll \frac{1}{h}\left(\frac{\varepsilon_0}{\mu_h}\right)^{1/2},$$

where c is the phase velocity of the electromagnetic waves in the liquid, h is the half width of the channel, ε_o is the

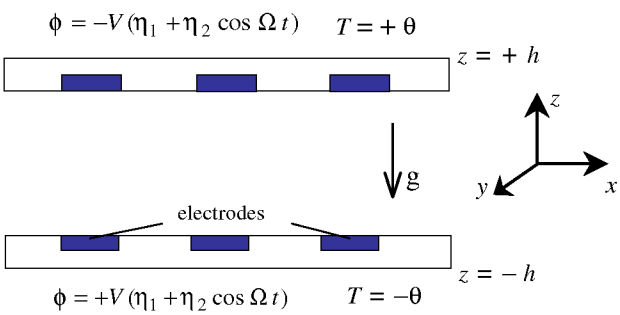

Figure 2. Physical configuration.

dielectric constant and μ_h is the magnetic permeability. For typical values[43],

$$\varepsilon_0 \sim 88.5 \times 10^{-12}\ \text{F/m}, \quad \mu_h \sim 4\pi \times 10^{-7}\ \text{G/m},$$

$$h \sim 10^{-1}\ \text{m and } c \sim 10^{8}\ \text{m/s},$$

and we have

$$\sigma_e \ll 0.1\ (\text{ohm}\cdot\text{m})^{-1}, \quad \Omega \ll 10^9\ \text{rad/s}.$$

Here we deal with a poorly conducting liquid, where $\sigma_e \sim 10^{-11} - 10^{-9}$ (ohm·m)$^{-1}$ and $\Omega \ll 10^9$ rad/s, so that we can easily neglect the induced magnetic field. In addition, we also neglect the Joule heat in the energy equation, the nonuniform polarization of the poorly conducting liquid and all electric charge injection. Under these approximations, the basic equations after making them dimensionless, using the scales h for length, $h^2/\ddot{\upsilon}$ for time, κ/h for velocity, $\rho_1\kappa\ddot{\upsilon}/h^2$ for pressure, θ_1 for temperature, $\varepsilon_e V/h_2$ for density of charge, V for potential, V/h for electric field, σ_0 for conductivity, $\ddot{\upsilon} = (\ddot{\mu}/\rho)$, $\ddot{\mu}$ is effective viscosity, are

$$\nabla\cdot\vec{q} = 0, \tag{15}$$

$$\frac{\partial\vec{q}}{\partial t} + \frac{1}{p_r}(\vec{q}.\nabla)\vec{q} = -\nabla p + \nabla^2\vec{q} + R_a T\hat{e} + G_e\rho_e\vec{E} - a^2\vec{q}, \tag{16}$$

$$P_r\frac{\partial T}{\partial t} + (\vec{q}.\nabla)\,T = \nabla^2 T, \tag{17}$$

$$\frac{\partial\rho_e}{\partial t} + \frac{1}{P_e}\nabla\cdot(\sigma\,\vec{E}) + \frac{1}{P_r}(\vec{q}\cdot\nabla)\rho_e = 0, \tag{18}$$

$$\nabla\cdot\vec{E} = \rho_e, \tag{19}$$

$$\vec{E} = -\nabla\varphi, \quad \vec{e} = (0, 0, 1), \quad \sigma = 1 + sT, \tag{20}$$

$$w = \frac{\partial w}{\partial t} = 0 \text{ at } z = \pm 1,$$

$$T = \pm 1 \text{ at } z = \pm 1, \tag{21}$$

$$\varphi = \mp(\eta_1 + \eta_2\cos\omega t) \text{ at } z = \pm 1,$$

where

$$R_a = \frac{g\beta\theta_1 h^3}{\lambda\ddot{\upsilon}}, \quad \sigma^2 = \frac{h^2}{k}, \quad P_r = \frac{\ddot{\upsilon}}{\kappa},$$

$$G_e = \frac{\varepsilon V^2}{\rho_1\kappa\ddot{\upsilon}}, \quad a^2 = \lambda\sigma^2, \quad P_e = \frac{\varepsilon_0\ddot{\upsilon}}{h^2\sigma_0}, \quad \omega = \frac{\Omega h^2}{\ddot{\upsilon}},$$

$$s = \alpha_h\theta_1, \quad \lambda = \frac{\upsilon}{\ddot{\upsilon}},$$

where R_a is the Rayleigh number, G_e is the electric analogue of Galileo number, P_r is the Prandtl number, P_e is the electric Prandtl number, ω is the dimensionless modulation frequency and s ($\ll 1$) is the nonuniformity of the electrical conductivity.

Basic state: We analyse the basic state of the system (eqs (15–21)) given by

$$\vec{q} = 0,\ T_b = T_b(z),\ \vec{E} = E_b(z, t)\hat{k},\ \rho_{eb} = (z, t).$$

The boundary conditions are

$$T_b = \pm 1,\ \phi = \mp(\eta_1 + \eta_2\cos\omega t) \text{ at } z = \pm 1.$$

From eqs (17) and (18), we get

$$T_b = +z, \tag{22}$$

$$E_b = \eta_1(1 - sz) + \eta_2\left[\left(1 - \frac{sz}{1 + w^2P_e^2}\right)\cos\omega t - \frac{wP_e sz}{1 + w^2P_e^2}\sin\omega t\right] + O(s^2). \tag{23}$$

$$\rho_{eb} = -\eta_1 s - \eta_2\frac{s}{1 + w^2P_e^2}(\cos\omega t + wP_e\sin\omega t) + O(s^2). \tag{24}$$

Perturbed state: To study the stability of the basic state (eqs (22)–(24)), we superimpose infinitesimal disturbances of the form

$$\vec{q} = \vec{q}',\ T = T_b + T',\ \rho_e = \rho_{eb} + \rho_e', \tag{25}$$

where prime denotes perturbed quantities.

Introducing perturbed quantities (eq (25)) into eqs (16)–(21), linearizing, eliminating pressure and assuming normal mode solutions of the form

$$\begin{pmatrix} \vec{q}_z' \\ T' \\ \rho_e' \end{pmatrix} = \begin{pmatrix} w(z, t) \\ \theta(z, t) \\ \rho_e(z, t) \end{pmatrix} e^{i\ell x}, \tag{26}$$

we get the following of linearized eqs (27)–(29), where w, θ, ρ_e are the amplitudes and ℓ is the horizontal wavenumber in the x-direction. We note that since E_b, g and ∇T are directed normal to the boundaries and hence the problem considered here is isotropic in the plane of the layer. The assumption $s \ll 1$ allows us to consider the electric field associated with charge redistribution due to electroconvection in the liquid to be much smaller than the externally applied electric field[43].

The linearized governing equations are:

$$\frac{\partial Dw}{\partial t} = D^2 w - R_a \ell^2 w - B \ell^2 \rho_e (\eta_1 + \eta_2 \cos \omega t) - a^2 Dw, \tag{27}$$

$$P_r \frac{\partial \theta}{\partial t} + w = D\theta, \tag{28}$$

$$P_e \frac{\partial \nabla^2 \phi}{\partial t} + \nabla^2 \phi = (\eta_1 + \eta_2 \cos \omega t) \frac{\partial \theta}{\partial z}, \tag{29}$$

where ℓ is the wavenumber, $D = \partial^2/\partial z^2 - \ell^2$, $B = G_e s$, $\rho_e = -\nabla^2 \phi$.

Boundary conditions for amplitudes on rigid isothermal plates are

$$w = 0, \quad \theta = 0, \quad z = \pm 1. \tag{30}$$

To study the stability of this system, first we have to obtain compatibility conditions. This is done in the next section using single-term Galerkin expansion procedure.

Galerkin method: In the single-term Galerkin expansion procedure, we assume

$$w(z, t) = A(t)(\omega_1)(z); \quad \theta(z, t) = C(t)\theta_1(z);$$
$$\phi(z, t) = E(t)\phi_1(z). \tag{31}$$

Substituting these in eqs (27)–(29) and eliminating A, C and E, we get

$$R_a = \frac{1}{P_r^2 \ell^2 \langle \theta_1 w_1^m \rangle \langle w_1 \theta_1^m \rangle} \left[(P_r \langle \theta_1 \theta_1^m \rangle - P_r \langle D\theta_1 \theta_1^m \rangle) \begin{pmatrix} P_r \langle D^2 w_1 w_1^m \rangle - \\ \langle D w_1 w_1^m \rangle - P_r a^2 \langle D w_1 w_1^m \rangle \end{pmatrix} - \frac{\begin{matrix} BP_e P_r \ell^2 (\eta_1 + \eta_2 \cos \omega t)^2 \\ \langle \nabla^2 \phi_1 w_1^m \rangle \langle w_1 \theta_1^m \rangle \left\langle \frac{\partial \theta_1}{\partial z} \phi_1^m \right\rangle \langle D w_1 w_1^m \rangle \langle \theta_1 \theta_1^m \rangle \end{matrix}}{\langle \nabla^2 \phi_1 \phi_1^m \rangle \begin{bmatrix} P_r \langle D^2 w_1 w_1^m \rangle \langle \theta_1 \theta_1^m \rangle + \langle D\theta_1 \theta_1^m \rangle \langle D w_1 w_1^m \rangle \\ - P_r^2 \langle \theta_1 \theta_1^m \rangle \langle D w_1 w_1^m \rangle \end{bmatrix}} \right]. \tag{32}$$

Criterion for the onset of EC: In this section we determine the conditions for the onset of EC using moment and energy methods.

Moment method: For the moment method, we set $m = 0$ in (32), and obtain

$$R_a = \frac{1}{P_e^2 \ell^2 \langle \theta_1 \rangle \langle w_1 \rangle} \left[(P_r \langle \theta_1 \rangle - P_r \langle D\theta_1 \rangle) \begin{pmatrix} P_r \langle D^2 w_1 \rangle - \\ \langle D w_1 \rangle - P_r a^2 \langle D w_1 \rangle \end{pmatrix} - \frac{BP_e P_r \ell^2 (\eta_1 + \eta_2 \cos \omega t)^2 \langle \nabla^2 \phi_1 \rangle \langle w_1 \rangle \left\langle \frac{\partial \theta_1}{\partial z} \right\rangle \langle D w_1 \rangle \langle \theta_1 \rangle}{\langle \nabla^2 \phi_1 \rangle [P_r \langle D^2 w_1 \rangle \langle \theta_1 \rangle + \langle D\theta_1 \rangle \langle D w_1 \rangle - P_r a^2 \langle \theta_1 \rangle \langle D w_1 \rangle]} \right]. \tag{33}$$

The boundary conditions are

$$w = 0, \quad \theta_1 = 0, \quad \varphi = \mp 1 \quad \text{at} \quad z = \pm 1. \tag{34}$$

Following the Galerkin technique[23], we choose the trail functions:

$$\omega_1 = \frac{1}{\sqrt{I_1}} \left[\frac{\cosh \ell z}{\cosh \ell} - \frac{\cos(\sqrt{\mu_1 - a^2 - \ell^2} z}{\cos \sqrt{\mu_1 - a^2 - \ell^2}} \right];$$

$$\theta_1 = \cos \frac{\pi}{2} z; \phi_1 = \frac{s}{2} - z - \frac{sz^2}{2}, \tag{35}$$

where

$$I_1 = \frac{\mu_1}{2(\ell^2 - \mu_1 + a^2)} (\ell^2 + \ell \tanh \ell - \ell^2 \tanh^2 \ell - \mu_1 + a^2).$$

The critical wavenumbers are determined from

$$\sqrt{\mu_1 - a^2 - \ell^2} \tan [\sqrt{\mu_1 - a^2 - \ell^2}] = -\ell \tanh \ell. \tag{36}$$

We note that this method is silent about the effect of electric Rayleigh number B on R_a because when θ_1 is even, $\langle D\theta_1 \rangle$ vanishes and when $D\theta_1$ is odd, $\langle \theta_1 \rangle$ itself vanishes in eq. (33). To predict the effect of electric Rayleigh number B on R_a, we use the energy method in the next section.

Energy method: For the energy method $m = 1$, then eq. (33) becomes

$$R_a = \frac{1}{P_r^2 \ell^2 \langle \theta_1 w_1 \rangle \langle w_1 \theta_1 \rangle}$$

$$\left[(P_r\langle\theta_1\theta_1\rangle - P_r\langle D\theta_1\theta_1\rangle)\begin{pmatrix} P_r\langle D^2 w_1 w_1\rangle - \\ \langle Dw_1 w_1\rangle - P_r a^2\langle Dw_1 w_1\rangle \end{pmatrix} - \frac{\begin{matrix} BP_e P_r \ell^2(\eta_1 + \eta_2\cos\omega t)^2\langle\nabla^2\phi_1 w_1\rangle\langle w_1\theta_1\rangle \\ \left\langle \frac{\partial\theta_1}{\partial z}\phi_1\right\rangle\langle Dw_1 w_1\rangle\langle\theta_1\theta_1\rangle \end{matrix}}{\begin{matrix} [\langle\nabla^2\phi_1\phi_1\rangle P_r\langle D^2 w_1 w_1\rangle\langle\theta_1\theta_1\rangle + \langle D\theta_1\theta_1\rangle\langle Dw_1 w_1\rangle \\ - P_r^2\langle\theta_1\theta_1\rangle\langle Dw_1 w_1\rangle] \end{matrix}} \right]. \quad (37)$$

We can integrate the integrals in eq. (37) using the trial functions (eq. (35)). Since the expression is lengthy it is omitted here, but it is numerically evaluated and the results are given below. The critical wavenumber is computed numerically by solving the transcendental eq. (36) for different values of B, P_r, P_e, ω and σ. Using this critical wavenumber, critical Rayleigh number R_{ac} is computed from eq. (37) and the results are given below.

The effect of unsteady electric field on EC in a poorly conducting, saturated, mushy layer made of dendrites of nano-size crystals is investigated using linear stability analysis within the EHD realm. Eigenvalue equations are derived using the calculus of variation. The compatibility condition is obtained from the eigenvalue equations using a single-term Galerkin expansion. The condition for the onset of EC is obtained using moment and energy methods. It is shown that the Rayleigh number R_a is independent of electric Rayleigh number B in the moment method. From this we conclude that moment method is inadequate in the present problem and hence eq. (37) for Rayleigh number is obtained using the energy method. The critical wavenumber ℓ_c is obtained numerically by solving the transcendental eq. (36) for $P_r = 1$, $P_e = 0.04$, $s = 0.01$, $w = 4$ and $t = 0$, 0.02, 0.01, 0.1, for different values of σ and B. Using these critical wavenumbers ℓ_c, the critical Rayleigh number R_{ac} is computed for the values of parameters given above and the results are predicted in Figures 3 *a* and *b*.

Figure 3 *a* pertains to the case heated from below as in Rayleigh–Benard convection for different values of electric Rayleigh number B and for fixed values of P_r, P_e, ω, s and σ. From Figure 3 *a*, it is clear that an increase in B decreases R_a and hence we conclude that the effect of increase in B is to augment convection. This instability physically results from interaction of electroconvective and thermo-gravity mechanisms as expected. Figure 3 *b* pertains to the case heated from below for various values of the porous parameter σ and for fixed values of B, P_r, P_e, ω and s. From Figure 3 *b* it is clear that an increase in σ increases R_a and hence the effect of increase in σ is to suppress convection. The Rayleigh number R_a is computed from eq. (37) for cooling from below and heating from above for different values of B and for fixed values of other parameters. The results are depicted in Figure 4.

From Figure 4, it is clear that an increase in B increases $-R_a$ for given values of the other parameters. From this we conclude that the effect of increase in B is to suppress EC. From Figures 3 *a* and 4, we conclude that the effect of electric field is to augment convection for heating from below, and suppressing convection for heating from above and cooling from below.

The electric Rayleigh number B is computed for different values of ω, and ℓ for $R_a = 0$ (i.e. absence of gravity) and for fixed values of other parameters. The results are given in Table 1.

Table 1 shows the behaviour of electroconvective thresholds in the absence of gravity, i.e. buoyancy-free case when $R_a = 0$. Only the electroconductive instability exists

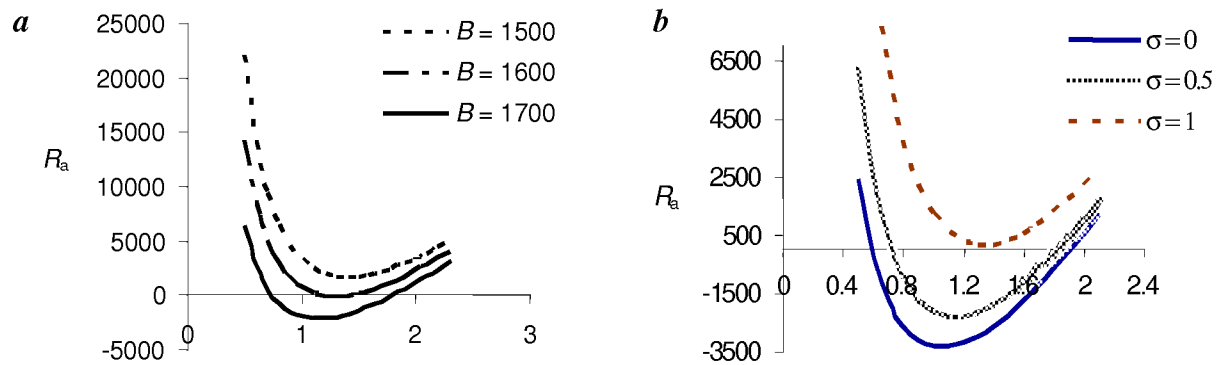

Figure 3. Rayleigh number R_a, for different values of (***a***) electric Rayleigh number B and (***b***) porous parameter σ.

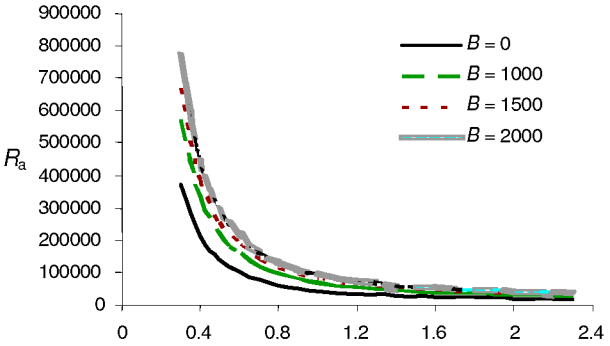

Figure 4. Rayleigh number $-R_a$ for different values of electric Rayleigh number B.

Table 1. Values of B for different values of ω and ℓ

	B				
ℓ	$\omega = 1$	$\omega = 2$	$\omega = 3$	$\omega = 4$	$\omega = 5$
0.1	605.01	621.87	651.35	695.82	759.09
0.3	592.61	609.12	638.00	681.55	743.53
0.6	574.96	590.97	618.99	661.25	721.37
0.9	563.19	578.88	606.33	647.72	706.62
1.2	569.67	585.54	613.30	655.17	714.74
1.5	602.07	618.84	648.18	692.43	755.39

and we see that the increase in the frequency ω increases the values of B, resulting in a destabilizing influence of modulation. Finally, we conclude that at finite modulation frequencies both stabilization and destabilization of the basic state are possible depending on the amplitude and frequency of the electric field.

Rayleigh–Taylor instability with porous lining

At present, only the linear RTI of the ablating plasma is extensively investigated, assuming the plasma to be initially at quiescent state and the following mechanisms are used to reduce the RTI growth rate.

(i) Gradual variation of density assuming plasma as an incompressible heterogeneous fluid without surface tension.
(ii) Assuming plasma as a compressible fluid without surface tension.
(iii) IFE target shell with porous foam layer.

Numerous experiments and numerical simulations of the above mechanisms except the foam, fit the following simple approximate formula for RTI growth rate at the ablation surface:

$$n = A\sqrt{\frac{\ell g}{1+\varepsilon_o \ell L}} - \beta \ell v_a, \tag{38}$$

where n is the growth rate, ℓ is the wavenumber of the perturbation, g is the acceleration due to gravity at the interface, ε_o is a constant multiplying the density gradient correction term, L is the density scale length at the ablation surface, A is the Atwood number, β is a constant multiplying the ablation stabilization, and v_a is the flow velocity across the ablation front, The first term on the right-hand-side of eq. (38) is the growth rate, N_b, for the classical RTI, i.e. incompressible inviscid fluid in the absence of porous lining, and the second term is the effect of compressibility. Choosing suitable values for the constants A, ε and β, one can fit the available data, as depicted in Table 2.

At present, the available work on the use of foam, to reduce the RTI growth rate, pertains to experimental work and no simple theoretical formula similar to eq. (38) is available. Therefore, Rudraiah *et al.*[49] found an analytical expression like eq. (38) using porous lining (i.e. non-deformable foam) on the ablative slab, where the porous material is made of foametal, aloxite or Invar alloys. When most materials are heated, they expand. But sometimes it is advantageous to have materials that ignore changes in temperature. In general, thermal expansion can have serious consequences. To overcome this problem, usually a material called Invar, an alloy of about one-third nickel and two-thirds iron, is used. This material has very low thermal expansion and ambient temperature, and it rarely swells. It was invented in 1920 by Invar, a French physicist, who got the Nobel Prize for this work.

Using Stokes and lubrication approximations valid when the wavelength of the instability is large compared to thickness of the layer, Rudraiah[50] derived an analytical formula for the RTI growth rate, considering dissipative incompressible plasma bounded on one side by a porous lining in the presence of surface tension γ at the interface:

$$n = \frac{1}{3}\ell^2\left(1-\frac{\ell^2}{B}\right) - \beta \ell v_a, \tag{39}$$

where $B = \delta h^2/\gamma$ is the Bond number, $\delta = g(\rho_p - \rho_f)$, γ is the surface tension, $\beta = 3\alpha\sigma/(4 + \alpha\sigma)$, $v_a = (4 + \alpha\sigma)/12(1 + \alpha\sigma)\ell(1 - \ell^2/B)$ is the velocity across the ablation front, n is the growth rate and ℓ is the wavenumber. We can see the similarities between eqs (38) and (39). The first term on the right-hand-side of eq. (39) is the growth rate n_b in the absence of porous layer, and for convenience we call it as the classical value for viscous incompressible fluid in the presence of surface tension, given by Babchin *et al.*[51].

From eq. (39) we get the maximum wavenumber, $\ell_m = \sqrt{B/2}$ obtained by setting $\partial\eta/\partial\ell = 0$ and the corresponding maximum growth rate, n_m, is given by

$$n_m = \frac{B(4+\alpha\sigma)}{48(1+\alpha\sigma)}. \tag{40}$$

Table 2. Values of A, ε_0 and β

Reference	A	ε_0	β
44	0.90	0.0	3.00
45	1.00	1.0	3.00
46	0.98	1.0	1.70
47	0.90	1.0	3.00
48	0.90	1.0	3.02

In the absence of porous lining the maximum wavenumber is $\ell_m = \sqrt{B/2}$ and the corresponding maximum growth rate is $n_{bm} = B/12$. Then we have

$$\frac{n_m}{n_{bm}} = \frac{(4+\alpha\sigma)}{4(1+\alpha\sigma)}. \tag{41}$$

From eq. (38), with $\beta = 3$ and $A = 0.9$, Takabe *et al.*[44] have obtained

$$(n_m)_{T_a} = 0.45(n_{bm})_{T_a}, \tag{42}$$

where suffix T_a refers to the results of Takabe *et al.*[44]. From eq. (42), Takabe *et al.*[44] concluded that the growth rate of RTI is reduced to 45% of the classical value $(n_{bm})_{T_a}$. From our eq. (41) with $\alpha = 0.1$ (aloxite material) and $\sigma = 4$, we get

$$n_m = 0.7857(n_m)_b. \tag{43}$$

From this we conclude that the mechanism of porous lining (non-deformable porous foam) reduces the growth rate of RTI to 78.57% of the classical value.

Our objective here is to know whether a suitable strength of magnetic field can reduce the RTI growth rate without considering the mechanism of porous lining. Also to derive a simple analytical formula analogous to the one given in eq. (38) or eq. (39).

Next the relevant boundary and surface conditions and approximations are given. The dispersion relation is then obtained using linear stability analysis. The formula for growth rate in the presence of magnetic field and absence of porous lining, analogous to eq. (39) is also derived. Some important conclusions are drawn.

Formulation of the problem

We consider a thin target shell in the form of a film of unperturbed thickness h filled with light, incompressible, viscous, electrically conducting plasma of constant density ρ_1 bounded on one side by a rigid surface and on the other side by an incompressible, heavy, viscous, electrically conducting plasma of density ρ_2 of an infinite extent, with an interface between the two plasma layers subject to a transverse magnetic field and surface tension

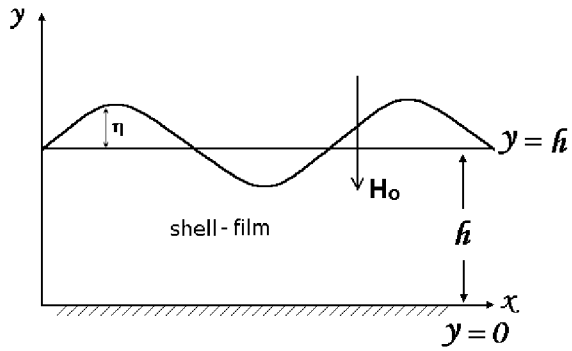

Figure 5. Physical configuration.

(Figure 5). This assumption on density is needed for RTI. The fluid within the shell sets in motion due to laser-accelerated ablative surface. At time t, the fluctuations of the interface are amplified and the local thickness becomes a function of the position and time t, and we have $y = h + \eta(x, t)$ where $\eta(x, t)$ is the surface displacement. We consider a rectangular coordinate system (x, y) as shown in the Figure 5, with x-axis parallel to the shell and y-axis normal to it and with $\eta(x, t)$ as the perturbed interface.

The basic equations for conducting, incompressible, viscous and electrically conducting plasma in the film are the conservation of momentum

$$\rho\left[\frac{\partial \vec{q}}{\partial t} + (\vec{q}\cdot\nabla)\vec{q}\right] = -\nabla p + \mu\nabla^2\vec{q} + \mu_h\,\vec{J}\times\vec{H}, \tag{44}$$

and the conservation of mass for an incompressible plasma.

$$\nabla\cdot\vec{q} = 0, \tag{45}$$

where $\vec{q} = (u, v)$ is the velocity, $\vec{J} = \sigma[\vec{E} + \mu_h\vec{q}\times\vec{H}]$ is the current density, $\nabla\times\vec{E} = -\mu_h\partial\vec{H}/\partial t$, $\nabla\cdot\vec{E} = 0, \nabla\cdot\vec{H} = 0$, $\vec{E}$ is the electric field, $\vec{H}$ is the magnetic field, μ is the viscosity, μ_h is the magnetic permeability and σ is the electrical conductivity of fluid. These equations have to be supplemented with suitable boundary and surface conditions. These equations are sufficient for our purpose since we deal with electrically conducting fluid of small conductivity σ, so that the induced magnetic field can be neglected in comparison with the applied magnetic field.

Here we deal only with linear two-dimensional RTI in continuum plasma, considering infinitesimally small disturbances superposed on the basic state. The basic state is quiescent and the interface is flat. Further, the following Stokes and lubrication approximations[27,51] will greatly simplify the analysis: (i) $\eta \ll h$. This assumption helps to neglect the variation of horizontal velocity u with respect to x. (ii) The Bond number $B = \delta h^2/\gamma \ll 1$, which implies

the gravitational effect is small compared to the surface tension effect, where γ is the surface tension and $\delta = (\rho_2 - \rho_1)$ is the normal stress. (iii) The Reynolds number $R = Uh^2/Lv \ll 1$, where v is the kinematic viscosity, which enables us to neglect inertial force because of very viscous fluid. (iv) The magnetic Reynolds number $R_m = \mu_h \sigma U_h \ll 1$, because of small electrical conductivity. This enables us to neglect induced magnetic field compared to the applied magnetic and electric fields. (v) The Strouhal number $S = L/t_o U \ll 1$, $L = \sqrt{\gamma/\delta}$ where t_o and U are the characteristic time and velocity which enable to neglect local acceleration in the momentum equation. These approximations, which are valid when the wavelength of the instability of the ablative surface is large compared to the thickness of the layer, are useful to neglect many terms, particularly nonlinear terms in the basic eq. (44). We also assume that heavy fluid bounding the lighter fluid is almost static because of creeping flow approximation which is needed to study RT-instability[51]. Under these approximations, the basic eq. (44) reduces to, after making the resulting equations dimensionless using the scales h for length, δh for pressure, $\delta h^2/\mu$ for velocity and $\mu/\delta h$ for time, the form

$$0 = -\partial p/\partial x + \partial^2 u/\partial y^2 - M^2 u, \tag{46}$$

$$0 = -\partial p/\partial y, \tag{47}$$

$$\partial u/\partial x + \partial v/\partial y = 0, \tag{48}$$

where $M = \mu_h h H_o \sqrt{\sigma/\mu}$ is the Hartmann number and H_o is the applied transverse magnetic field. These equations have to be solved using the following boundary and surface conditions. The no-slip condition at the rigid surface is

$$u = v = 0 \quad \text{at} \quad y = 0. \tag{49}$$

No shear at the free surface is

$$\partial u/\partial y = 0 \quad \text{at} \quad y = 1. \tag{50}$$

The dynamic condition is

$$p = -\eta - \frac{1}{B}\frac{\partial^2 \eta}{\partial x^2} \quad \text{at} \quad y = 1. \tag{51}$$

For linear analysis, the kinematic condition is

$$v = \partial\eta/\partial t \quad \text{at} \quad y = 1. \tag{52}$$

Dispersion relation

Solving eq. (43) and using the conditions in eqs (49) and (50), we get

$$u = \frac{P}{M^2}\left[\frac{ChM(1-y)}{ChM} - 1\right], \; ChM = \cosh M, \; P = \frac{\partial p}{\partial x}. \tag{53}$$

Integrating eq. (48) with respect to y from 0 to 1 and simplifying, we get

$$v(1) = \frac{MChM - ShM}{M^3 ChM}\frac{\partial^2 p}{\partial x^2}, \; ShM = \sinh M. \tag{54}$$

From eq. (52), using normal mode solution of the form $\eta = \eta_o e^{i\ell x + nt}$ and using eqs (51) and (54), we get the dispersion relation of the form

$$n = n_0 - \beta \ell v_a,$$

where

$$v_a = \frac{(M - \tanh M)\,\ell\,(1 - \ell^2/B)}{M^3}, \tag{55}$$

$$\beta = \frac{M^3 - 3(M - \tanh M)}{3(M - \tanh M)},$$

n is the growth rate, ℓ is the wavenumber, B is the Bond number, and

$$n_0 = \frac{\ell^2}{3}(1 - \ell^2/B), \tag{56}$$

obtained from eq. (55) in the limit of $M \to 0$, and for convenience we call it the classical value. Note that for comparison purpose, v_a is used both in eqs (38) and (55), but they are different.

Equation (55) clearly shows that the effect of magnetic field is to reduce the growth rate of RTI considerably compared to the one in the absence of the magnetic field. The physical reason for this reduction is that the transverse magnetic field suppresses the flow by converting the kinetic energy into magnetic energy.

A self-consistent analytical approach is used to study linear RTI of an ablatively laser-accelerated target filled with an incompressible electrically conducting viscous plasma, in the presence of a transverse magnetic field. The RTI growth rate formula given by eq. (55) is analogous to the one given by eq. (38) for compressible fluid, and eq. (39) for porous lining.

Setting $n = 0$ in eq. (55), we obtain the cut-off wavenumber ℓ_{ct} above which RTI mode is stabilized and is found to be

$$\ell_{ct} = \sqrt{B}. \tag{57}$$

The maximum wavenumber ℓ_m obtained from eq. (55) by setting $\partial n/\partial \ell = 0$ is

$$\ell_m = \sqrt{B/2} = \ell_{ct}/\sqrt{2}. \tag{58}$$

Equations (57) and (58) are true even in the absence of magnetic field (i.e. $M = 0$) given by eq. (56) and for convenience we call them as classical results. The maximum growth rate, n_m, for the corresponding ℓ_m given by eqs (55) and (56) is

$$n_m = \frac{B}{4}\left(\frac{1}{3} - \Delta\right), \quad \Delta = \frac{M^3 - 3(M - \tanh M)}{3M^3}, \tag{59}$$

Table 3. Variation of G_m with M

Hartmann number M	Maximum growth rate G_m
0.01	0.99996
0.10	0.99602
1.00	0.71522
10.00	0.02700
100.00	0.00030

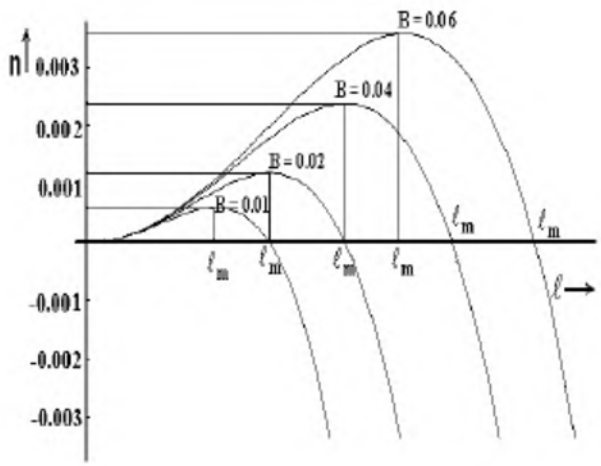

Figure 6. Growth rate n versus wavenumber ℓ for $M = 1$ and for different bond numbers B.

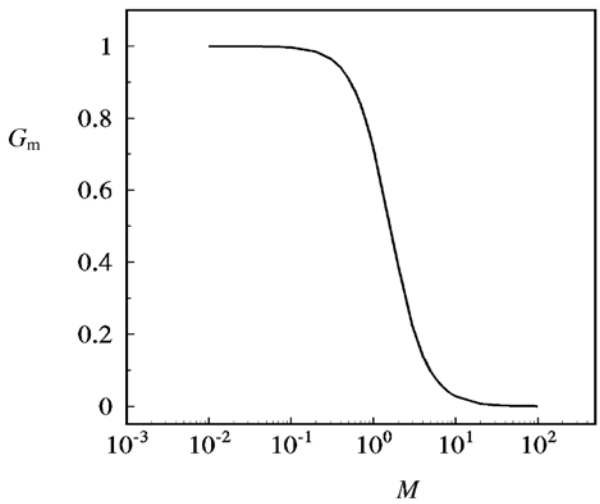

Figure 7. Ratio of maximum growth rate G_m versus M.

$$n_{om} = B/12. \tag{60}$$

From these, we get the ratio of maximum growth rate n_m to n_{om}, given by

$$G_m = n_m/n_{om} = 3(M - \tanh M)/M^3. \tag{61}$$

Equation (55) is plotted in Figure 6 for the growth rate n versus the wavenumber ℓ for $M = 1$ and for different values of B. We see that the perturbations of the interface having a wavenumber smaller than ℓ_{ct} are amplified when $\delta > 0$ (i.e. $\rho_1 < \rho_2$) and the growth rate decreases with a decrease in B, implying increase in surface tension. That is, increase in surface tension makes the interface more stable. Similar behaviour is observed even for $M = 10$ and it was found that an increase in M decreases the growth rate considerably. To know the amount of reduction in the growth rate by magnetic field compared to that in the absence of magnetic field, eq. (61) is numerically computed for different values of M ranging from 10^{-2} to 10^2. The results are given in Table 3 and are also plotted in Figure 7 with G_m versus M. We see that the decrease in the growth rate compared to the classical one is steep for M in the range 10^{-1} to 10^1 and the ratio G_m becomes independent of M for values $M > 10$, tending to the value of 0.0003. For $M = 1$, we find that $G_m = 0.71522$, that is, the maximum growth rate is reduced to 71.52% of the classical value n_{om}. However, at $M = 10$, we find that the maximum growth rate is reduced by 97.3% of the classical value n_{om}. Similarly, for $M = 100$, we find that the maximum growth rate is reduced to 99.97% of the classical value n_{om}. From this, we conclude that an increase in the value of magnetic field M, reduces considerably the growth rate compared to the classical value. This information is useful in the extraction of IFE efficiently, by maintaining the symmetry of the target.

1. Ling, R. Y., *Ferroelectrics*, 1990, **102**, 215.
2. Neumann, R. E., Xu, Q. C., Kumar, S. and Cross, L. E., *Cross Ferroelectrics*, 1990, **102**, 259.
3. Rudraiah, N., Venkatachalappa, M. and Malashetty, M. S., Oberbeck convection through vertical porous stratification. *Proc. Indian Acad. Sci.* (*Math. Sci.*), 1982, **91**, 17–37.
4. Chandrasekhar, S., *Hydrodynamics and Hydromagnetic Stability*, Cambridge Univ. Press, 1961.
5. Rudraiah, N., Asymptotic methods in magnetoconvection. *Indian J. Pure Appl. Maths.*, 1997, **26**, 969–1003.
6. Rudraiah, N., Nonlinear interaction of magnetic field and convection in three dimensional motion. *Astron. Soc. Jpn.*, 1981, **33**, 721–738.
7. Rudraiah, N. and Shivakumara, I. S., *Int. J. Heat Mass Transfer*, 1984, **27**, 1825–1836.
8. Pearson, J. R. A., On convection cells induced by surface tension. *J. Fluid Mech.*, 1958, **4**, 489–500.
9. Rudraiah, N. and Friedrich, R., Periodic and chaotic behaviour of highly truncated spectral models for cellular convection in fluids and porous media. *Proceedings of the International Congress of Theoretical and Applied Mechanics*, Denmark, Aerg, 1984.

10. Rudraiah, N. and Ramachandra Murthy, V., Effects of non-uniform temperature gradient an Coriolis force on Benard–Marangoni instability. *Acta Mech.*, 1986, **61**, 37–50.
11. Rudraiah, N. and Prasad, V., Effect of Brinkman layer on the onset of Marangoni convection in a fluid-saturated porous layer. *Acta Mech.*, 1998, **27**, 235–246.
12. Rudraiah, N., Ramachandra Murthy, V. and Chandna, O. P., *Int. J. Heat Mass Trasnfer*, 1985, **28**, 1621–1624.
13. Rudraiah, N., Chandna, O. P. and Garg, M. R., *Indian J. Technol.*, 1986, **24**, 279–284.
14. Rudraiah, N. and Shekhar, G. N., Effect of nonuniform temperature gradient on convection in magnetic fluids. *Proceedings of Canadian Conference on Continuum Mechanics and Applications*, Simon Fraser University, Canada, 1988.
15. Rudraiah, N. and Siddheshwar, P. G., Effect of nonuniform basic temperature gradient on the onset of Marangoni convection in fluid with suspended particles. *J. Aerospace Sci. Technol., Fr.*, 2000, **48**, 517–523.
16. Rudraiah, N., Krishnamurthy, B. S., Jalaja, A. S. and Desai, T., Effect of magnetic field on the growth rate of Rayleigh–Taylor instability of a laser accelerated thin ablative surface. *Laser Part. Beam*, 2004, **22**, 1–5.
17. Nagashree, M. S., Effect of Coriolis force on electroconvection. M Phil thesis, Bangalore Univ., 2001.
18. Hemalatha, Electroconvection in porous media. M Phil thesis, Bangalore Univ., 2001.
19. Radhakrishna, Effect of cross diffusion electroconvection. M Phil thesis, Bangalore Univ., 2001.
20. Sethuram, H. R., Double diffusive electroconvection. M Phil thesis, Bangalore Univ., 2001.
21. Premini Nair, Marangoni electroconvection, M Phil thesis, Bangalore Univ., 2001.
22. Rudraiah, N. and Kaloni, P. N., Marangoni electroconvection in the presence of an electrofield in a fluid heated from above. *Acta Mech.*, 2003, **166**, 217–229.
23. Rudraiah, N., Nonlinear convection in a porous media with convective acceleration and viscous force. *Arab. J. Sci. Eng.*, 1984, **9**, 153–167.
24. Rudraiah, N., Siddheshwar, P. G. and Masuoka, T., Nonlinear convection in porous media. *J. Porous Media*, 2003, **6**, 1–32.
25. Rudraiah, N., Int. Conference on porous media and their application in science, engineering and industry, Hawaii, USA, 1996, vol. 30.
26. Rudraiah, N., Krishnamurthy, B. S. and Masuoka, T., *Proc. Indian Acad. Sci.* (*Math. Sci.*), 1997, **107**, 213–220.
27. Rudraiah, N., Mathad, R. D. and Hameeda, B., *Curr. Sci.*, 1997, **72**, 391–395.
28. Rudraiah, N., Instabilities of importance in the manufacture of nano and smart materials. In *Modelling of Nano and Smart Materials*, Book Paradise, Bangalore, 2003.
29. Rudraiah, N. and Prema, S., Rayleigh–Taylor instability in a thin film bounded by a porous layer. *Natl. Acad. Sci. Lett.*, 1998, **21**.
30. Rudraiah, N. and Shanthakumar, M., On the stability of the flow of stratified rotating superposed fluids. *Astron. Soc. Jpn.*, 1974, **26**, 221–239.
31. Rudraiah, N. and Shanthakumar, M., Stability of a stratified rotating conducting gas over a rotating conducting fluid. *Vignana Bharathi*, 1976, **2**, 30–40.
32. Plouraboué, F. and Hinch, E. J., Kelvin Helmoltz instability in Hele–Shaw cell. *Phys. Fluids*, 2002, **14**, 922–929.
33. Richtmyer, R. D., Taylor instability in shock acceleration of compressible fluids. *Common Pure Appl. Math.*, 1960, **13**, 297–319.
34. Mikaelian, K. O., Turbulent energy at accelerating and shocked interface. *Phys. Fluids*, 1990, **A2**, 592–598.
35. Kaviany, M., *Principles of Heat Transfer in Porous Media*, Springer Verlag, 1991.
36. Nield, D. A. and Began, A., *Convection in Porous Media*, Springer Verlag, 1999.
37. Beavers, G. S. and Joseph, D. D., *J. Fluid Mech.*, 1967, **30**, 197–207.
38. Rudraiah, N., Coupled parallel flows in a channel and a bounding porous medium of finite thickness. *ASME J. Fluid Eng.*, 1985, **107**, 322–329.
39. Rudraiah, N., Venkatachalappa, M. and Siddalinga Prasad, M., In *Modelling of Nano and Smart Materials*, Book Paradise, Bangalore, 2003.
40. Turnbull, R. J., Electro convective instability with a stabilizing temperature gradient – II experimental results. *Phys. Fluids*, 1968, **11**, 2597–2603.
41. Lee, C. O., Kim, M. U. and Kim, D. I., Electrohydrodynamic cellular bulk convection induced by a temperature gradient. *Phys. Fluids*, 1972, **15**, 789–795.
42. Lee, C. O., Thermal instability of slightly conducting liquid layer in a vertical electric field. Proceedings of the 5th International Heat Transfer Conference, Tokyo, 1974, vol. 3, pp 173–177.
43. Smorodin, B. L. and Velarde, M. G., Electro thermo convective instability of an ohmic liquid layer in an unsteady electric field. *J. Electrost.*, 2000, **48**, 261–277.
44. Takabe, H., Mima, K., Montierth, L. and Morse, R. L., Self consistent growth rate of the Rayleigh–Taylor instability in an ablatively accelerating plasma. *Phys. Fluids*, 1985, **28**, 3676–3682.
45. Lindl, J. D., *Phys. Plasma*, 1995, **2**, 3933–3941.
46. Betti, R., Goncharov, V. N., McCroy, R. L. and Verdovi, C. P., *Phys. Plasma*, 1995, **2**, 3844.
47. Kilkenny, J. D. *et al.*, *Phys. Plasma*, 1994, **1**, 1374–1386.
48. Kanuer, J. P. *et al.*, *Phys. Plasma*, 2000, **7**, 338–345.
49. Rudraiah, N. *et al.*, *IJAME*, 2003, **8**.
50. Rudraiah, N., *Fusion Science and Technology*, Special Issue on 2nd IAEA Technical Committee Meeting, 2003, vol. 43, pp. 1–5.
51. Babchin, A. J. *et al.*, Nonlinear saturation of Rayleigh–Taylor instability. *Phys. Fluids*, 1983, **26**, 3159–3161.

ACKNOWLEDGEMENTS. N.R. is indebted to William Mong Engineering Research Fund Committee of Management, Faculty of Engineering, The University of Hong Kong for awarding him this research fellowship. N.R. acknowledges the financial support of ISRO under project no. 10/2/300. The work of C.-O.N. was supported by the Research Grants Council of the Hong Kong Special Administrative Region, China.

Received 15 September 2003; accepted 31 January 2004